Front. Phys. 13(2), 137302 (2018)
https://doi.org/10.1007/s11467-017-0736-0

RESEARCH ARTICLE

# Strong interlayer coupling in phosphorene/graphene van der Waals heterostructure: A first-principles investigation

**Xue-Rong Hu, Ji-Ming Zheng†, Zhao-Yu Ren‡**

*Institute of Photonics & Photo-technology, National Key Laboratory of Photoelectric Technology and Functional Materials (Culture Base), National Photoelectric Technology and Functional Materials & Application of Science and Technology International Cooperation Base, Northwest University, Xi'an 710069, China*
*Corresponding authors. E-mail: †zjm@nwu.edu.cn, ‡rzy@nwu.edu.cn*
*Received July 19, 2017; accepted October 26, 2017*

Based on first-principles calculations within the framework of density functional theory, we study the electronic properties of phosphorene/graphene heterostructures. Band gaps with different sizes are observed in the heterostructure, and charges transfer from graphene to phosphorene, causing the Fermi level of the heterostructure to shift downward with respect to the Dirac point of graphene. Significantly, strong coupling between two layers is discovered in the band spectrum even though it has a van der Waals heterostructure. A tight-binding Hamiltonian model is used to reveal that the resonance of the Bloch states between the phosphorene and graphene layers in certain $K$ points combines with the symmetry matching between band states, which explains the reason for the strong coupling in such heterostructures. This work may enhance the understanding of interlayer interaction and composition mechanisms in van der Waals heterostructures consisting of two-dimensional layered nanomaterials, and may indicate potential reference information for nanoelectronic and optoelectronic applications.

**Keywords** strong coupling, vdW heterostructure, DFT calculations, tight-binding Hamiltonian model

**PACS numbers** 73.22.-f, 73.90.+f

Frontiers of Physics

## 1 Introduction

Two-dimensional (2D) layered nanomaterials are significant ingredients in nanoelectronics [1, 2] and optoelectronics [3–5] because of their unique mechanical, electronic, optical, and thermal properties, which are not found in their bulk counterparts. In addition to graphene, there are a series of new 2D materials with various advantageous properties such as hexagonal boron nitride (hBN) [6], transition metal dichalcogenides [7], and phosphorene [8], which have recently attracted a large amount of attention and been developed for various potential applications because of their high electron mobility [9, 10], increasing direct band gap with a decreasing number of layers [11], high anisotropy [12], and a strain-tuneable band gap [13]. However, every material has its limitations, such as the absence of a band gap in graphene [14], low mobility in $MoS_2$ [15], and instability in phosphorene [16].

In order to solve the abovementioned problems, a 2D van der Waals (vdW) heterostructure has been proposed as an effective method building new nanostructures [17] that will preserve the distinctive properties of each material and potentially adjust and control the properties of the final heterostructure. It has been reported that couping phosphorene with stable graphene [18] or hBN [19] and even phosphorene suboxide [20] and organism $TiL_4$ [21] can protect phosphorene and tune the carrier dynamics and optical properties. The phosphorene/graphene heterostructure has been proposed as an anode material for rechargeable Li batteries according to a first-principles study [22]. The phosphorene/$MoS_2$ heterostructure is a type-II semiconductor as an ultraviolet photodetector [23]. In addition, the black-phosphorus/blue-phosphorus heterostructure is predicted to be used in solar energy conversion [24].

Traditionally, weak coupling exists in vdW heterostructures, but recent experiments reported the existence of a strong coupling in a vdW heterostructure [25]. In this paper, we use first-principles calculations to investigate this issue, and a vertically stacked phosphorene/graphene heterostructure is studied as an example. The results show that although the unique properties of

graphene and phosphorene are well preserved after the formation of a vdW heterostructure, various band gaps are also observed at the band cross site. We analyze the interactions between layers and use a simple tight-binding Hamiltonian to explain the origin of these band gaps in such heterostructures. In addition, we found that strong coupling originates from the resonance between the Bloch waves of different layers at some K points when three conditions are met: close energy, symmetry matching, and a large overlap between waves of the two layers. This conclusion may enhance our understanding of the properties of vdW heterostructures.



## 2 Methodology

We implemented electronic properties calculations for the graphene/phosphorene heterostructure using the Vienna *ab initio* simulation package (VASP) [26] based on density functional theory (DFT) in the field of first-principles calculations. Generalized gradient approximation (GGA) proposed by Perdew–Burk–Ernzerhof (PBE) [27] was used for the exchange and correlation potential. The projector augmented wave potential (PAW) [28, 29] was used to treat the ion-electron interactions. As is known from previous theoretical calculations, the van der Waals interaction must be accounted for between bilayers to properly describe the properties of phosphorene by a dispersion-corrected DFT method (optB88-vdW) [30], with which we calculated band structures and work functions. A $3 \times 7 \times 1$ Gamma-centered grid was used in the Brillouin zone sampling of the relaxation calculation, and $6 \times 14 \times 1$ and a plane-wave cutoff energy of 500 eV was adopted in all the calculations. The thickness of the vacuum spacing was 30 Å to avoid image interaction owing to the periodicity. The structure was relaxed until the residual force on each atom was less than $10^{-4}$ eV/Å.

## 3 Structural and electronic properties

### 3.1 Geometrical structure

In our calculation, a $3 \times 1$ phosphorene is stacked on top of a $4 \times 1$ graphene supercell to form the unit cell of a heterostructure, as shown in Fig. 1(a). The optimized lattice constants are $a = 9.87$ Å and $b = 4.09$ Å. The strain induced by the lattice mismatch is approximately 1.4% (mean absolute strain along the $a$ axis is $\varepsilon_{11} = 0.7\%$ and along the $b$ axis is $\varepsilon_{22} = 3.5\%$) in either graphene or phosphorene. In Fig. 1(b), the evolution of the total energy is shown as a function of the interlayer distance. The most stable interlayer distance is 3.49 Å. Layers of vdW heterostructures are easy to slide with respect to adjacent layers. Therefore, using the optimized interlayer distance, we translated graphene with respect to phosphorene along zigzag and armchair directions to analyze the relation between configurations and electronic properties, and to obtain the most stable configuration. In Fig. 1(c), it is obvious that the energy is slightly periodic along the armchair direction, and the highest energy is only approximately 0.1 eV higher than the lowest energy and is nearly constant along the zigzag direction. The inset shows the configurations with minimum and maximum total energy.

### 3.2 Band structure

Figure 2(a) shows the band spectrum of the heterostructure, in which the black line indicates the bands of the configurations with minimum total energy, and the gray line indicates the bands of configurations with maximum total energy. It is evident that the black lines and gray lines almost coincide, implying that stacking patterns have little influence on the band spectrum of a heterostructure. In contrast with a monolayer band spectrum, the superposition of the bands of monolayer graphene (red line) and monolayer phosphorene (green line) are also shown in Fig. 2(b). One can observe that the band spectrum of the heterostructure coincides with the spectrum of superposition of each monolayer's bands for most of the lines. This means that the electronic properties of phosphorene and graphene are preserved in general after composing a heterostructure, which is a significant property in vdW heterostructures.

However, two features can be observed. One is that small band gaps appear at the Dirac point of graphene. In Fig. 2(c), we show the details of the band structures of the configurations at enlarged scales near the Fermi level, from $\Gamma$ to $Y$. As for graphene, the Dirac point is just on the Fermi level independent of strain, but after composing with phosphorene, the Dirac point shift upward about 0.01 eV above the Fermi level and opens a band gap about 0.03 eV. This results from the weak interactions between the $p_z$ orbital of the phosphorene and the $\pi$ cloud of graphene. Where the phosphorene and graphene bands cross, there are also small band gaps that were not discovered or reported in previous literature [18, 31]. (We will discuss the origin of these gaps at the end of the paper.)

The other feature is that the Dirac point of graphene is shifted to the middle of the $\Gamma Y$ lines owing to Brillouin zone folding, as depicted in Fig. 2(d). The black solid line indicates the Brillouin zone of graphene, and the smaller red line indicates the heterostructure. The graphene Brillouin zone folds into the red square after combining with the heterostructure. The dark blue solid line indicates the final folding result, in which the Dirac

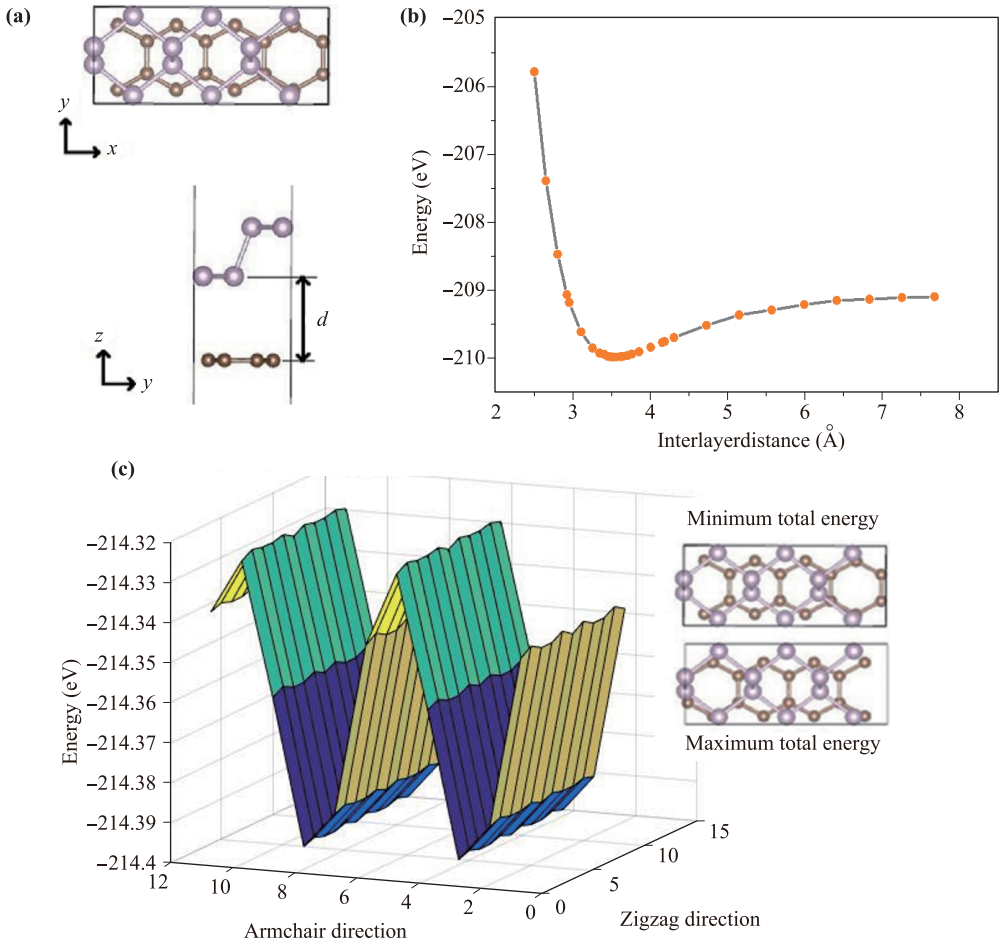


**Fig. 1** **(a)** Top and side view of phosphorene/graphene heterostructure. **(b)** Total energy as a function of interlayer distance. **(c)** Total energy variation trend with distinct displacements. We mesh the unit cell of the heterostructure using $10 \times 10$ grids. Along the armchair direction, the unit length is $0.1b$; along the zigzag direction, the unit length is $0.1a$, ($a = 9.87$ Å, $b = 4.09$ Å). Inset shows configurations with minimum and maximum total energy.

point is located approximately in the middle of the $\Gamma$ and $Y$ symmetry points.

### 3.3 Strain effect

Pristine phosphorene without strain is a semiconductor with a direct band gap of about 1.00 eV. Under a strain state (delete the graphene from the heterostructure), it changes to an indirect semiconductor with a smaller band gap of 0.21 eV, as shown in Fig. 2(b). This demonstrates that interlayer coupling is not the main reason for the gap variation, and that the band gap of phosphorene is very sensitive to strain. Compared to the previous results, one can find that both uniaxial and biaxial strains up to $\sim 5\%$ result in an increase in the band gap, and the direct feature is also preserved [32, 33]. In this work, a large decrease in the band gap occurs. This can be attributed to the anisotropic strain on the monolayer phosphorene. As we stated above, the strain induced by the lattice mismatch is around 1.4% (mean absolute strain) in either graphene or phosphorene. The strain in one direction ($b$ axis) is largely compressed and is relatively small in another direction ($a$ axis). That is, the values of the strain are not equal in the two directions. We test the band gap variations when isotropic biaxial strains of 1% and 2% are applied to monolayer phosphorene, and find that the band gaps are 0.98 eV and 1.09 eV, respectively. This is in accordance with the previously reported results. However, the reason why the band gap change so great is still needed further study.

### 3.4 Band alignment

Figure 3 depicts the band alignment and work function. The horizontal green lines represent the VBM (valence band maximum) and CBM (conduction minimum) of the monolayer or the heterostructure. The red cross indicates the Dirac point of graphene, and the blue numbers are

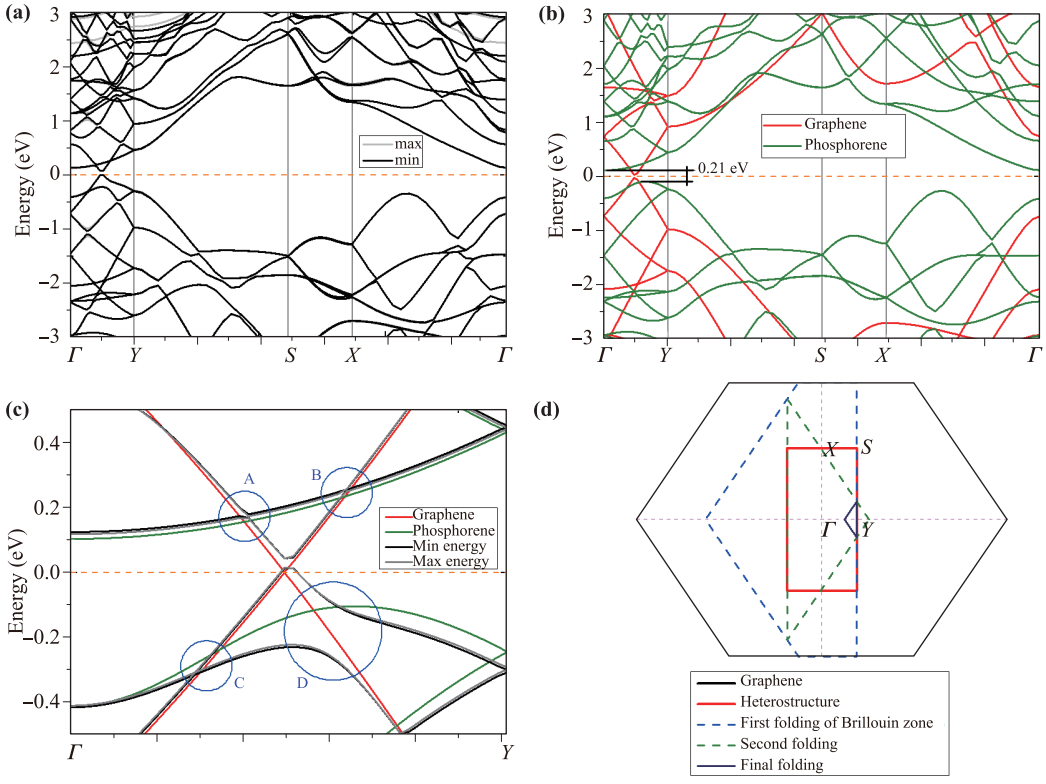


**Fig. 2** Band structure of **(a)** the heterostructure with minimum and maximum energy, and **(b)** superposition of bands of monolayer graphene and monolayer phosphorene (in green line) under strain states. **(c)** Enlarged figure of band structure of heterostructure along $\Gamma$ to $Y$. Circles A, B, C, and D highlight positions where bands cross. **(d)** Schematic of Brillouin zone folding.

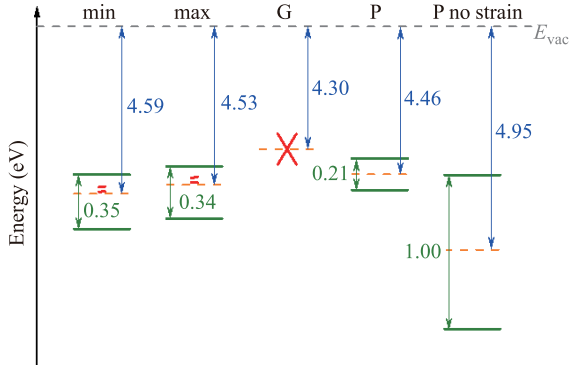


**Fig. 3** Band alignment of phosphorene/graphene heterostructure with minimum energy and maximum energy, and monolayer graphene and phosphorene with 1.4% in-plane strain and pristine monolayer phosphorene.

the work function. All values presented are aligned with respect to the vacuum level. We can see that the work function of strained graphene is 4.30 eV, which is lower than that of pristine graphene, at approximately 4.62 eV. Similarly, the strained phosphorene has a work function of about 4.46 eV, which is also lower than the value of pristine phosphorene, at about 4.95 eV, based on our results. Strain will cause a total energy increase, leading to the upward movement of the Fermi level. Phosphorene has a work function that is 0.16 eV larger than that of graphene. As a result, electrons transfer from graphene to phosphorene, making the Dirac point of graphene now higher in position than that of the Fermi level of the heterostructure. It is also evident that heterostructures have larger work functions than those of either strained graphene or strained phosphorene. Weak vdW interactions can increase the attraction between layers and lower the Fermi level of the heterostructure with respect to that of monolayer graphene and phosphorene.

### 3.5 Strong coupling

Figure 2(c) shows an enlarged figure of the band structure of the heterostructure along $\Gamma$ to $Y$. The band cross points are highlighted by circles. One can find that there are two types of band cross points. Points circled by A, B, and C indicate where only small gaps are opened, while points circled by D indicate where a large gap occurs. In Fig. 4, the contribution of a single layer's states to the heterostructure's Bloch states is indicated by green

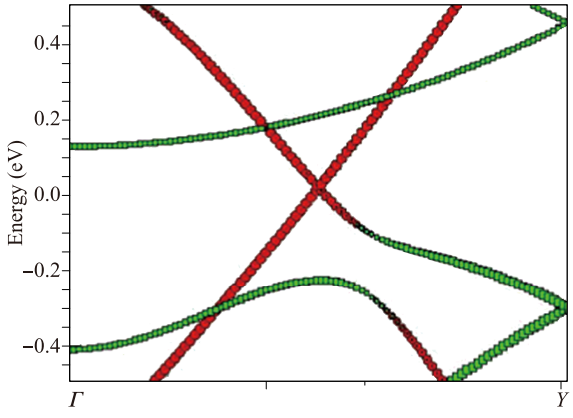


**Fig. 4** Enlarged figure of band structure of heterostructure along $\Gamma$ to $Y$. At each $K$ point, the composition of Bloch wave is indicated by red circles as a wave function from carbon atoms and green squares from phosphorous atoms. Sizes of squares and circles represent the magnitude of contribution.

squares and red circles, respectively, and the sizes of the squares and circles represent the magnitude of contribution. It can be seen that bands of the heterostructure are composed mainly of the single layer's states at most of the $K$ points, and their compositions switch where the single layer's bands cross in different materials. It is usually reported that weak electron coupling exists in a vdW heterostructure. This does not change the layout of a single layer's bands. However, we observe not only weak coupling but also strong coupling at some $K$ points where the heterostructure's bands change significantly.

Comparing the band structure of the heterostructure with that of the superposition of two single layers, we find two types of gaps where VB (valence band) and CB (conduction band) of monolayer phosphorene and graphene cross. In order to explain this phenomenon, we introduce a tight-binding model of two one-dimensional atomic chains with different densities of atoms: an upper chain with two atoms in one unit cell, and a bottom chain with three. The vdW interactions between the chains is significantly weaker than the atomic covalent bonds inside the chains. The Hamiltonian of the system is expressed:

$$H = H_1 + H_2 + H_{\text{int}} = \frac{t_k}{2} \sum_{i,j} C_i^+ C_j,$$

where the total Hamiltonian $H$ is composed of three parts: $H_{1/2}$ represents the upper/bottom single atom chain, and $H_{\text{int}}$ represents the interaction between two chains. $t_k$ are the hopping items, which have different values representing the different coupling strengths between atoms in the system. ($t_1 = -1.0$ is used for the hopping inside the upper chain, $t_2 = -1.5$ is used for the bottom chain, and $t_{12}$ is used to represent the vdW interaction between the chains.) $C_i^+/C_j$ represent the creator and annihilator of electrons.

Figure 5 shows the details of the band structures, in which different values of interchain hopping items are used. When $t_{12}$ equals zero, two types of bands without interaction are observed in Fig. 5(b), where the black line indicates the bands of the upper chain, and the red line indicates the bands of the bottom chain. When a small $t_{12}$ is introduced, there are two types of band gap opening. One is observed at the $K$ points where the first black and red bands (higher in energy position) cross each other, while the other is at the $K$ points where the second bands (lower in energy position) cross. For the first type, where a stronger interaction exists between the two chains, larger gaps open at these $K$ points. However, for the second type, no apparent band-gap opening can be observed when $t_{12}$ increases. The panels below the band structures are composed of the highest band's Bloch states at each $K$ point. In the left panel, a sudden change in the plot means weak coupling between chains. The sudden change always occurs in the second type of band cross, where no apparent band gaps open. By contrast, in the middle and right panels, Bloch states at $K$ points around $\pm 0.2$ show states apparently mixing between the two chains, which indicates strong coupling between different chains and leads to a large band gap.

With regard to the wave mechanism, the upper chain's Bloch wave can interact strongly with the Bloch wave of the bottom chain only when three conditions are met: close energy, symmetry matching, and large overlap between the waves of the two chains. At the $K$ points of band crossing, two Bloch waves have the same energy and $K$ vector, so the maximum of the wave overlap is the key to inducing strong coupling. This occurs at the band crossing shown in Fig. 5(a), where the bonding states of the upper chain interact strongly with the antibonding states of the bottom chain, while the antibonding states of the upper chain have weak coupling with the antibonding states of the bottom chain.

Returning to the heterostructure we are studying, there are four band-cross points along the $\Gamma$–$Y$ axis. Although the Bloch states of each layer have the same energy and $K$ vector at the crossing points, they can still be classified into two types. In Fig. 6, we show the calculated Bloch waves of each layer at four band-crossing $K$ points. It can be observed that the graphene layer shows bonding states along the Y direction and antibonding states along the $X$ direction in A and D, while it shows bonding states along the $X$ direction and antibonding states along the $Y$ direction in B and C. At the same time, phosphorene shows bonding states along both the $X$ and $Y$ directions and antibonding states along the $Z$ direction in A and B, while it shows bonding states along the X, $Y$, and $Z$ directions in C. It is only D that

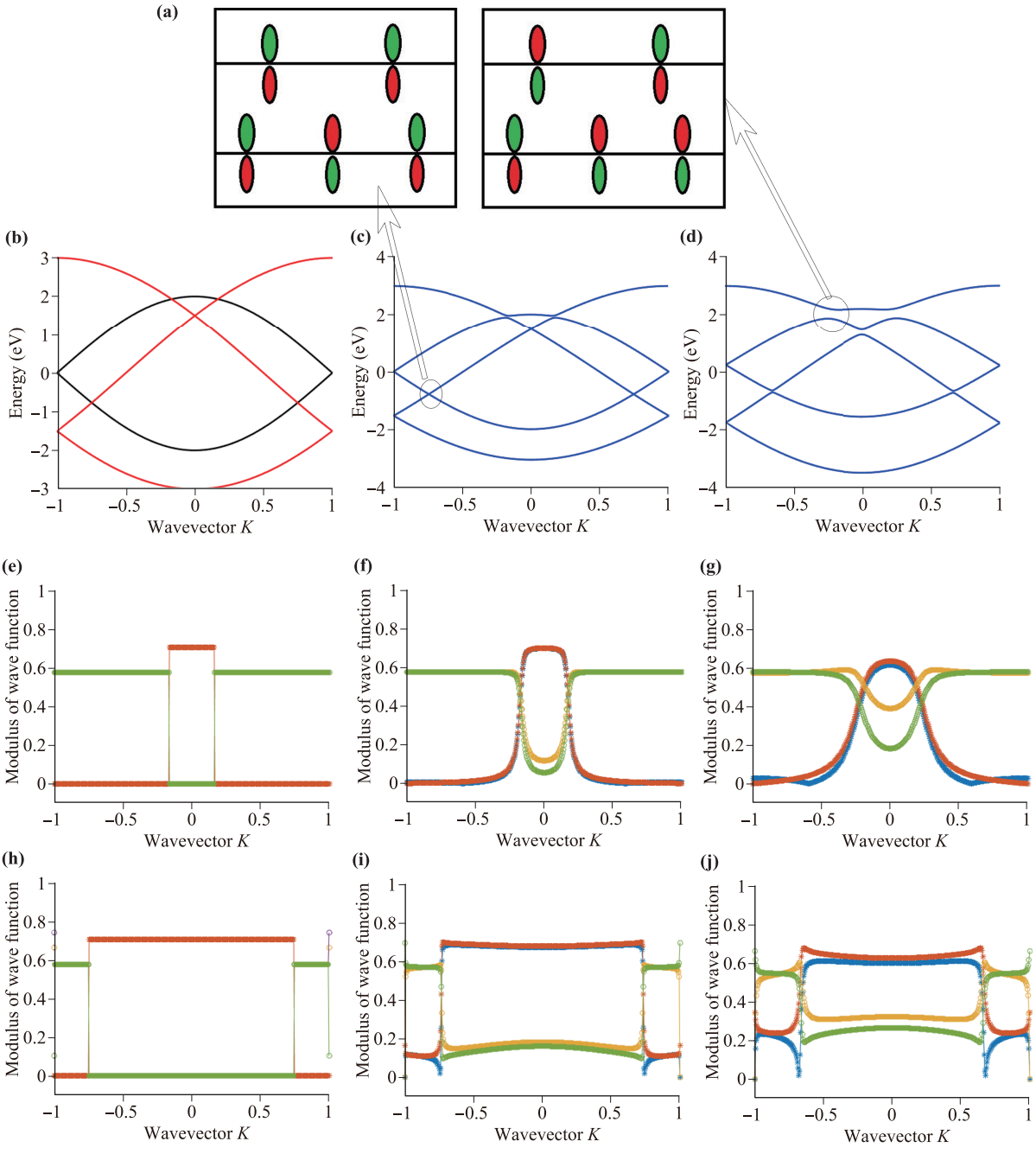


**Fig. 5** **(a)** Schematic figure of the layout of wave functions of atom chains at band-crossing points. the red and green colors represent different phases of wave functions. **(b–d)** Band structures of the tight-binding model with different $t_{12}$ values: 0, −0.1, and −0.5. Modulus of the wave function of **(e–g)** the fifth (highest) band and **(h–j)** the second band under different $t_{12}$, corresponding to their band spectrums on the upper panels.

shows bonding states along the $Y$ and $Z$ directions and antibonding along the $X$ direction, matching the characteristics of the graphene Bloch wave in D. This will give a strong resonance between graphene and phosphorene and induce a large gap in the band spectrum. At other points, the Bloch waves of two layers have different layouts, which leads to weak coupling and small gaps.

## 4 Conclusions

We studied the structural and electronic properties of phosphorene/graphene heterostructures by using first-principles calculations. We found that the total energy of the heterostructure was slightly periodic along

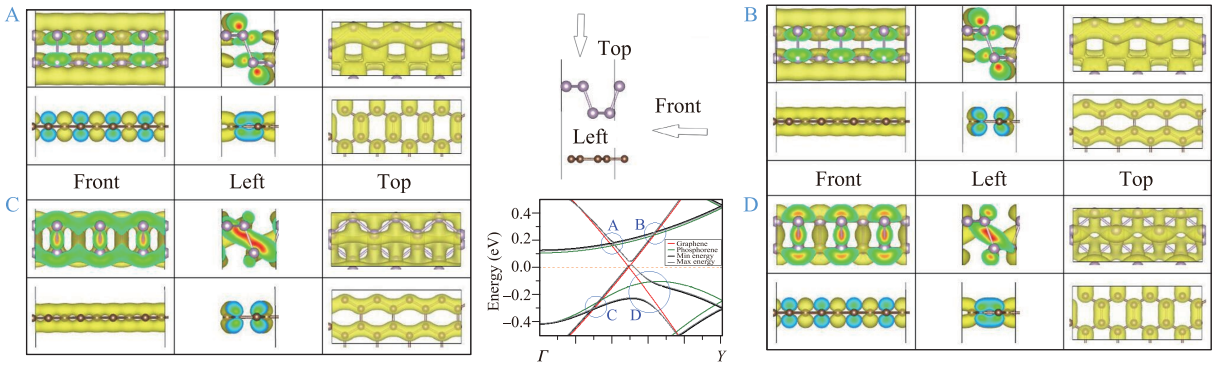


**Fig. 6** Four groups of wave functions: A, B, C, and D, corresponding to four $K$ points in the middle picture, where the single layer's bands cross. In each group, the upper and bottom three panels are three views of the wave functions of phosphorene and graphene at corresponding $K$ points.

the armchair direction and nearly constant along the zigzag direction. The properties of graphene and phosphorene were preserved after contacting, except in band gaps at certain $K$ points, and charges transferred from graphene to phosphorene, causing the Fermi level of the heterostructure to shift downward with respect to the Dirac point of monolayer graphene. Significantly, both strong and weak coupling between two layers were observed in the band spectrum. Using a tight-binding Hamiltonian model, we found that the resonance between the Bloch waves of different layers was strong when three conditions were met. Two waves should have similar energy, matched symmetry, and a large overlap. At the $\Gamma$–$Y$ axis in the Brillouin zone, only one site among all four band-crossing points satisfied all three conditions and led to strong coupling and a large band gap. The others met only some of the conditions, gave rise to weak coupling between layers, and induced small band gaps. Our results can be helpful for the further understanding of the interlayer interaction and composition mechanism in van der Waals heterostructures, and can serve as potential reference information for nanoelectronic and optoelectronic applications.

**Acknowledgements** Thanks to Professor Zhipei Sun (Aalto University, Finland) for valuable discussions. This work was supported by the International Cooperative Program (Grant No. 2014DFR10780), the National Natural Science Foundation of China (Grant No. 61275105), the Natural Science Foundation of Shaanxi Province (Grant No. 2014JM2-1008), and the State Key Laboratory of Transient Optics and Photonic Technology 2015 Annual Open Fund (Grant No. SKLST200915).

## References

1. C. J. Shih, Q. H. Wang, Y. Son, Z. Jin, D. Blankschtein, and M. S. Strano, Tuning on-off current ratio and field-effect mobility in a $MoS_2$-graphene heterostructure via Schottky barrier modulation, *ACS Nano* 8(6), 5790 (2014)
2. Y. Deng, Z. Luo, N. J. Conrad, H. Liu, Y. Gong, S. Najmaei, P. M. Ajayan, J. Lou, X. Xu, and P. D. Ye, Black phosphorus-monolayer $MoS_2$ van der Waals heterojunction p-n diode, *ACS Nano* 8(8), 8292 (2014)
3. J. Lu, J. Yang, A. Carvalho, H. Liu, Y. Lu, and C. H. Sow, Light–matter interactions in phosphorene, *Acc. Chem. Res.* 49(9), 1806 (2016)
4. J. Lu, A. Carvalho, J. Wu, H. Liu, E. S. Tok, A. H. C. Neto, B. Özyilmaz, and C. H. Sow, Enhanced photoresponse from phosphorene–phosphorene-suboxide junction fashioned by focused laser micromachining, *Adv. Mater.* 28, 4090 (2016)
5. M. M. Furchi, A. Pospischil, F. Libisch, J. Burgdörfer, and T. Mueller, Photovoltaic effect in an electrically tunable van der Waals heterojunction, *Nano Lett.* 14(8), 4785 (2014)
6. A. Pakdel, Y. Bando, and D. Golberg, Nano boron nitride flatland, *Chem. Soc. Rev.* 43(3), 934 (2014)
7. Q. H. Wang, K. Kalantar-Zadeh, A. Kis, J. N. Coleman, and M. S. Strano, Electronics and optoelectronics of two-dimensional transition metal dichalcogenides, *Nat. Nanotechnol.* 7(11), 699 (2012)
8. L. Li, Y. Yu, G. J. Ye, Q. Ge, X. Ou, H. Wu, D. Feng, X. H. Chen, and Y. Zhang, Black phosphorus field-effect transistors, *Nat. Nanotechnol.* 9(5), 372 (2014)
9. F. Xia, H. Wang, and Y. Jia, Rediscovering black phosphorus as an anisotropic layered material for optoelectronics and electronics, *Nat. Commun.* 5, 289 (2014)
10. H. Liu, A. T. Neal, Z. Zhu, Z. Luo, X. Xu, D. Tománek, and P. D. Ye, Phosphorene: An unexplored 2D semiconductor with a high hole mobility, *ACS Nano* 8(4), 4033 (2014)
11. M. Buscema, D. J. Groenendijk, G. A. Steele, H. S. J. van der Zant, and A. Castellanos-Gomez, Photovoltaic

effect in few-layer black phosphorus PN junctions defined by local electrostatic gating, *Nat. Commun.* 5, 4651 (2014)

12. V. Tran, R. Soklaski, Y. Liang, and L. Yang, Layer-controlled band gap and anisotropic excitons in few-layer black phosphorus, *Phys. Rev. B* 89(23), 235319 (2014)
13. A. S. Rodin, A. Carvalho, and A. H. Castro Neto, Strain-induced gap modification in black phosphorus, *Phys. Rev. Lett.* 112(17), 176801 (2014)
14. F. Schwierz, Graphene transistors, *Nat. Nanotechnol.* 5(7), 487 (2010)
15. R. Ganatra and Q. Zhang, Few-layer $MoS_2$: A promising layered semiconductor, *ACS Nano* 8(5), 4074 (2014)
16. J. O. Island, G. A. Steele, H. S. J. van der Zant, and A. Castellanos-Gomez, Environmental instability of few-layer black phosphorus, *2D Materials* 2 (1), 011002 (2015)
17. A. K. Geim and I. V. Grigorieva, Van der Waals heterostructures, *Nature* 499(7459), 419 (2013)
18. J. E. Padilha, A. Fazzio, and A. J. da Silva, Van der Waals heterostructure of phosphorene and graphene: Tuning the Schottky barrier and doping by electrostatic gating, *Phys. Rev. Lett.* 114(6), 066803 (2015)
19. T. Hu and J. Hong, Anisotropic effective mass, optical property, and enhanced band gap in BN/phosphorene/BN heterostructures, *ACS Appl. Mater. Interfaces* 7(42), 23489 (2015)
20. J. Lu, A. Carvalho, W. Jing, H. Liu, E. S. Tok, A. H. C. Neto, B. Özyilmaz, and C. H. Sow, Phosphorene: Enhanced photoresponse from phosphorene-phosphorene-suboxide junction fashioned by focused laser micromachining, *Adv. Mater.* 28(21), 4164 (2016)
21. Y. Zhao, H. Wang, H. Huang, Q. Xiao, Y. Xu, Z. Guo, H. Xie, J. Shao, Z. Sun, and W. Han, Surface coordination of black phosphorus for robust air and water stability, *Angew. Chem. Int. Ed.* 55(16), 5003 (2016)
22. G. C. Guo, D. Wang, X. L. Wei, Q. Zhang, H. Liu, W. M. Lau, and L. M. Liu, First-principles study of phosphorene and graphene heterostructure as anode materials for rechargeable Li batteries, *J. Phys. Chem. Lett.* 6(24), 5002 (2015)
23. J. Dai and X. C. Zeng, Bilayer phosphorene: effect of stacking order on bandgap and its potential applications in thin-film solar cells, *J. Phys. Chem. Lett.* 5(7), 1289 (2014)
24. L. Huang and J. Li, Tunable electronic structure of black phosphorus/blue phosphorus van der Waals p-n heterostructure, *Appl. Phys. Lett.* 108(8), 083101 (2016)
25. H. Fang, C. Battaglia, C. Carraro, S. Nemsak, B. Ozdol, J. S. Kang, H. A. Bechtel, S. B. Desai, F. Kronast, A. A. Unal, G. Conti, C. Conlon, G. K. Palsson, M. C. Martin, A. M. Minor, C. S. Fadley, E. Yablonovitch, R. Maboudian, and A. Javey, Strong interlayer coupling in van der Waals heterostructures built from single-layer chalcogenides, *Proc. Natl. Acad. Sci. USA* 111(17), 6198 (2014)
26. G. Kresse and J. Furthmüller, Efficiency of *ab-initio* total energy calculations for metals and semiconductors using a plane-wave basis set, *Comput. Mater. Sci.* 6(1), 15 (1996)
27. J. P. Perdew, K. Burke, and M. Ernzerhof, Generalized gradient approximation made simple, *Phys. Rev. Lett.* 77(18), 3865 (1996)
28. G. Kresse and D. Joubert, From ultrasoft pseudopotentials to the projector augmented-wave method, *Phys. Rev. B* 59(3), 1758 (1999)
29. P. E. Blöchl, Projector augmented-wave method, *Phys. Rev. B* 50(24), 17953 (1994)
30. J. Klimeš, D. R. Bowler, and A. Michaelides, Van der Waals density functionals applied to solids, *Phys. Rev. B* 83(19), 195131 (2011)
31. Y. Cai, G. Zhang, and Y. W. Zhang, Electronic properties of phosphorene/graphene and phosphorene/hexagonal boron nitride heterostructures, *J. Phys. Chem. C* 119(24), 13929 (2015)
32. B. Sa, Y. L. Li, J. Qi, R. Ahuja, and Z. Sun, Strain engineering for phosphorene: The potential application as a photocatalyst, *J. Phys. Chem. C* 118(46), 26560 (2014)
33. R. Fei and L. Yang, Strain-engineering the anisotropic electrical conductance of few-layer black phosphorus, *Nano Lett.* 14(5), 2884 (2014)